

Mast Cells Populate the Corneoscleral Limbus: New Insights for Our Understanding of Limbal Microenvironment

Alessandra Micera,¹ Katerina Jirsova,² Graziana Esposito,¹ Bijorn Omar Balzamino,¹ Antonio Di Zazzo,³ and Stefano Bonini³

¹Research Laboratories in Ophthalmology, IRCCS-Fondazione Bietti, Rome, Italy

²Laboratory of the Biology and Pathology of the Eye, Institute of Biology and Medical Genetics, First Faculty of Medicine, Charles University and General University Hospital in Prague, Prague, Czech Republic

³Ophthalmology Research Unit, University Campus Bio-Medico, Rome, Italy

Correspondence: Stefano Bonini, Campus Bio-Medico University of Rome, Via Alvaro del Portillo 200, Rome 00128, Italy; s.bonini@unicampus.it.

Received: June 19, 2019

Accepted: December 14, 2019

Published: March 24, 2020

Citation: Micera A, Jirsova K, Esposito G, Balzamino BO, Di Zazzo A, Bonini S. Mast cells populate the corneoscleral limbus: new insights for our understanding of limbal microenvironment. *Invest Ophthalmol Vis Sci.* 2020;61(3):43. <https://doi.org/10.1167/iovs.61.3.43>

PURPOSE. Although stem cell activity represents a crucial feature in corneal and ocular surface homeostasis, other cells populating this region and the neighboring zones might participate and influence local microenvironment. Mast cells, the long-lived and tissue-sited immune cells, have been previously reported in corneoscleral specimens. Herein, mast cells were investigated in corneoscleral tissues and related to microenvironment protein expression.

METHODS. Twenty-six (14 male/12 female; older than 60 years) human corneoscleral specimens were sectioned for light and fluorescent immunostaining (CD45, p63, Ck-3/7/12/19, tryptase/AA1, and chymase/CC1). Corneal, limbal, and conjunctival squares were produced for molecular and biochemical analysis. Statistical comparisons were carried out by ANOVA.

RESULTS. Toluidine blue staining identified metachromatic intact or degranulated mast cells in the area below the palisades' Vogt (Ck-3/12-positive epithelium and underneath p63 immunoreactivity). Tryptase immunoreactivity was observed close to palisades' Vogt, whereas no specific signal was detected for chymase. Tryptase/AA1 transcripts were quantified in limbal and conjunctival RNA extracts, whereas no specific amplification was detected in corneal ones. Few mediators were overexpressed in limbal extracts with respect to corneal (Neural cell adhesion molecule (NCAM), Intercellular adhesion molecule 3 (ICAM3), Brain-derived Neurotrophic factor (BDNF), and neurotrophin 3 (NT3); $P < 0.00083$) and conjunctival (NCAM, ICAM3, and NT3; $P < 0.05$) protein extracts. A trend to an increase was observed for Nerve Growth Factor (NGF) in limbal extracts ($P > 0.05$).

CONCLUSIONS. The specific observation of tryptase phenotype and the interesting protein signature of microenvironment (adhesion molecules, growth factors, and neurotrophins), known to partake mast cell behavior, at least in other areas, would provide additional information to better understand this crucial zone in the framework of ocular surface healthiness.

Keywords: mast cells, corneoscleral limbus, ocular surface, microenvironment, NGF, protein signature

The corneoscleral limbus is a crucial region of the ocular surface housing stem cells/progenitors for continuous self-renewal of corneal cells throughout the lifetime.¹⁻⁶ Any kind of insult at the stem cell niches can affect significantly homeostasis and healthiness of the ocular surface, triggering defect of reepithelization or even failures in the follow-up of routine surgery.⁷⁻¹⁰ Several in vitro and ex vivo approaches have been developed so far for counteracting and/or treating stem cell deficiency to increase the outcome of surgery in case of limbal defects.^{8,11-14} Corneoscleral limbus is also characterized by intensive innervation and vascularization of this microenvironment that is highly populated by structural

and immune cells engaging critical dealings with stem cells.⁸ Altogether, an incessant cell-to-mediator crosstalk sustains local homeostasis and drives a proper healing to protect stem cell activity when required.¹⁵ Of interest, few old and recent studies highlighted the distribution of mast cells in normal corneoscleral tissues.¹⁶⁻¹⁸ Mast cells are long-living cells of the innate immune system, residing strategically in tissue exposed to the external environment and interacting with the surrounding tissue microenvironment.¹⁹ Besides the pivotal role in type I and IV (delayed) hypersensitivity, most mast cell activities are still largely unknown. Mast cells work as sentinels (gatekeepers) encompassing active tasks

in (innate) immunity, angiogenesis, wound healing, cancer, fibrosis, and other inflammatory/degenerative routes.^{19–22} The concept around mast cell activity has been improved in the past decade with the observation that these cells respond to both immunoglobulin E (IgE)–dependent and IgE-independent stimuli, sustaining the homeostatic activities and justifying their presence in the nervous system.^{23–25} In line with the recent findings and progress in personalized medicine, corneoscleral mast cells require further investigation.

Herein, we sought to localize and characterize phenotypically the mast cells in corneoscleral limbus as well as ascertain the protein signature of this peculiar microenvironment.

MATERIALS AND METHODS

Human Specimens

The study encompasses an overall 2015–2017 period. Human corneoscleral tissues were obtained from a small group of specimens not suitable for transplantation ($n = 26$; 60- to 77-year-old donors; Biology and Pathology of the Eye, Prague, Czech Republic). All procedures for corneoscleral tissue handling followed the standards of the Ethics Committees of the General Teaching Hospital and the First Faculty of Medicine of Charles University, Prague, Czech Republic. Overall, experimental procedures were performed in accordance with the Association for Research in Vision and Ophthalmology guidelines and adherent to the tenets of the Declaration of Helsinki concerning human subject contribution.

Only corneoscleral specimens not suitable for transplantation and showing intact epithelium (from cornea to limbus and conjunctiva) as well as stored for fewer than 4 days in Optisol/Epilife medium (Bausch & Lomb, Rochester, NY, USA) were selected for the study. Specimens were cut in squares and quickly frozen in Optic Cutting Temperature (OCT) compound (TissueTek; Leica, Heidelberg, Germany) or snap-frozen. All specimens were sent by courier to the laboratory, according to the triple packaging/shipping procedure.

Reagents

Unless specified below, sterile RNase-free plasticware and molecular/analytical-grade reagents were from Starlab (Ahrensburg, Germany), ICN (Costa Mesa, CA, USA), SERVA (Weidelberg, Germany), Sigma-Aldrich (Milan, Italy), and Euroclone (Milan, Italy) unless otherwise specified in the text. Ultrapure RNase-free MilliQ-Grade water was provided daily (Direct Q5 apparatus; Millipore, Vimodrone, Milan, Italy) for biochemical studies and for molecular analysis as Diethyl pyrocarbonate (DEPC)-treated and autoclave aliquots.

Light and Fluorescent Microscopy

OCT-embedded corneoscleral specimens were cut in 5- μ m serial sections (CM3050 cryostat; Leica Microsystems, Rijswijk, Netherlands), placed onto glass slides (BDH, Milan, Italy), quickly air-dried, and stored until specific staining. Sections were postfixed in cold 0.05% buffered formaldehyde and used as reported below. Sections from paraffin-embedded specimens were used for basal histology after

dewaxing and rehydrating steps (downscaling Et-OH steps until water and buffered saline).

Basal Histology. Sections were stained/counter stained with 1% toluidine blue in 1% saline (TB), hematoxylin and eosin (HE), or cresyl violet (all from Bio-Optica, Milan, Italy), and digital images were produced with a direct E400 Eclipse light microscope (Nikon, Tokyo, Japan).

Immunohistochemistry and Immunofluorescence. Antigen retrieval (0.05% trypsin-EDTA solution, 2 minutes) and avidin-blocking/permeabilizing (1% BSA and 0.5% Triton X100 in PBS, 5 minutes) steps were performed before probing with specific monoclonal/polyclonal antibodies (Table 1). The Avidin-Biotin Complex technique (Vectastain Elite kit; ABC-HRP Kit; Vector Laboratories, Burlingame, CA, USA) coupled to 3,3'-Diaminobenzidine (DAB) (Dako, Carpinteria, CA) developing was used for immunohistochemistry. Hematoxylin (Bio-Optica) counterstaining was used to better visualize the positive brown cells. Specifically, for primary antibodies developed in mouse, a mouse-on-mouse biotinylated anti-mouse Ig kit (MOM; Vector Laboratories) was used to discriminate immunoreactivity. The secondary Cy2 (green)–Cy3 (red)–Cy5 (blue) conjugated species-specific antibodies (1:150–1:300; donkey; Jackson ImmunoResearch, Europe Ltd, Suffolk, UK) were used for immunofluorescent labeling. Depending on the double-fluorophore mixture, nuclear counterstaining was performed with propidium iodide (PI; Molecular Probes, Eugene, OR, USA) or 4',6-diamidino-2-phenylindole (DAPI) (Sigma-Aldrich, St. Louis, MO, USA). Confocal high-resolution acquisitions were carried out on an inverted E2000U Eclipse microscope equipped with benchtop laser system and digital image C1 software (Nikon). Channel series were performed using the negative controls (omission of primary antibodies) to reduce not specific signals. Epifluorescence acquisitions were also carried out with a direct Ni E200 Eclipse microscope equipped with NIS Elements Image software (Nikon), with the following objectives: $\times 10$ /dry 0.75 dic m/n2, $\times 20$ /0.45 NA, $\times 40$ /0.60 NA, and finally $\times 60$ /1.4 oil/immersion. To provide quantitative results, positive cells were evaluated by direct counting in the limbal area (700 \times 500 μ m per section; $n = 3$ per sample). Representative digital images were assembled by Adobe Photoshop 7.0 software (Abacus Concepts, Irvine, CA, USA) and no changes with respect to original acquisitions were carried during panel assembling.

Tissue Microdissection and Biomolecular Analysis

Specific microdissection was performed to provide portions suitable for 30- μ m radial or tangential cross-sectioning. Briefly, corneoscleral specimens were dissected into three portions: four limbal, four corneal, and four conjunctival squares, all belonging to the same corneoscleral specimen. Cutting activity was carried out under a dissecting stereomicroscope (SMZ645; Nikon) equipped with cold-light optic fibers (PL2000 photonic; Axon, Vienna, Austria), under the supervision of an expert pathologist. Limbal zone was defined by the end of the Bowman's layer, at the level of vascularized connective tissue. Peripheral cornea was defined 2 mm from limbal landmark, characterized by the avascular cornea. Each of these three portions was cut into cubes of approximately 1 \times 1.5 \times 2.5 mm by a scalpel, and pooled samples (four squares for specimen) were directly extracted in lysis buffer (mirVana PARIS RNA and Native Protein Purification kit; ThermoFisher Scientific, Waltham,

TABLE 1. Antibodies and Primers

Immunofluorescence					
Target	Dilution	Host	Specificity	Source	
Ck3	1:100	Mouse	Corneal marker	Dako	
Ck12	1:100	Mouse	Corneal/limbal marker	Dako	
Ck7	1:100	Mouse	Limbal/conjunctival marker	Dako	
Ck19	1:100	Mouse	Conjunctival marker	Dako	
CD45	1:200	Mouse	Pan-leukocytes	Santa Cruz	
Tryptase/AA1	1:100	Mouse	Mast cell marker	Santa Cruz	
Chymase/CC1	1:100	Mouse	Mast cell marker	Santa Cruz	
cKit/CD117	1:50	Goat	Mast cell marker	R&D Systems	
FcεRI	1:70	Sheep	High-affinity IgE receptor	R&D Systems	
Western Blotting					
Target	Dilution	Host	Code	Expected Band	Source
NCAM1	1:1000	Mouse	ab-230724	100–45 kDa	Abcam
ICAM3	1:1000	Rabbit	CD50/sc-656269	90–132 kDa	Santa Cruz
BDNF	1:700	Rabbit	N-20/sc-546	15–30 kDa*	Santa Cruz
NT3	1:1500	Mouse	sc-80250	35 kDa	Santa Cruz
NGF	1:700	Rabbit	H-20/sc-548	15–30 kDa*	Santa Cruz
Molecular Analysis					
Target	Accession	Sequence (Left Primer)	Tm/Amplicon		
Hu tryptase (AA1)	BC028059.1	Gatcatcgtgcaccaca	60°C/185 bps		
Hu chymase1	BC103975.1	Agagctgaagctggggagat	60°C/100 bps		
Hu GAPDH	BC013310	Gaaggggtcattgatggcaac	63°C/100 bps		
Hu H3	NM005324	Gtctgcaggctggcatagaag	61°C/100 bps		
Hu 18S	NR003286	Ggagagggagcctgagaaac	60°C/100 bps		
cKit/CD117	KT326922	Ttctaccaggtggcaaaag	60°C/100 bps		
FcεRI	NM002001	Ctgaagccttctggtct	60°C/100 bps		

Amplification profile: hot start activation (95°C/15 minutes); 39 cycles: denaturation at 94°C/10 seconds, annealing at 58°C/15 seconds, extension at 72°C/10 seconds; melting curve recording 55°C to 95°C with one fluorescence reading every 0.5°C; further extension 75°C/5 minutes.

* Both precursor and mature form can be detectable under 4% to 12% SDS-PAGE separation.

MA, USA). Subsequently, two-thirds of the extract was used for the biochemical analysis and one-third of the extract was devoted to the molecular analysis. Opening quantification analysis was carried out for protein (3-μL extracts) and total RNA (1.5-μL extracts; A280 program; limit as >1.8 ratio) by using a spectrophotometer for small volumes (A1000 Nanodrop; Celbio, Milan, Italy).

Total Protein Analysis, Chip-Based Protein Array, and Related Validations

For chip-based hybridization, a total of 21 samples (7 for each subgroup) were loaded in customized G-series glass slides (14 identical subarrays per slide, with 60 biomarkers; Ray-Biotech, Norcross, CA, USA). Briefly, normalized protein extracts (350 ng/mL for array well) were processed according to a previously reported procedure.²⁶ Spin-dried slides were acquired in a GenePix 4400 Microarray platform (Molecular Devices LLC, Sunnyvale, Silicon-Valley, CA). Normalized fluorescent intensity (FI) data were calculated by the GenePix Pro 6.0 software (Axon Instruments; Molecular Devices). Interassay normalization was guaranteed by the presence of multiple internal controls for each subarray. The minimum sensitivity ranged between 3.8 and 56 pg/mL. Fold changes from array analysis were validated by Western blotting (NCAM, ICAM3, and NT3; Table 1) and ELISA (NGF and BDNF). For Western Blotting (WB) analysis, normalized protein extracts (30 μg) were preheated in loading buffer (75°C/5 min), electrophoresed under reducing conditions

(4%–12% precast resolving SDS-PAGE gels; 130 V/frontline; MiniProtean3 apparatus; Bio-Rad Laboratories Inc, Hercules, CA), transferred to membranes (0.22 μm Hybond; GE Healthcare, Buckinghamshire, UK; 13 V/45 min; semidry Trans-Blotting apparatus; Bio-Rad), and finally stained with the high-sensible Pierce reversible protein stain kit for nitrocellulose membranes (ThermoFisher Scientific). Samples showing an overexpression of bands specific for albumin, IgGs, and/or fibronectin were treated with the bead-based depletion kit (GE Healthcare) before loading. Immunoblots were probed according to a standard procedure, and developing was performed by horseradish peroxidase-conjugated antibodies and chemiluminescent substrate (ThermoFisher Scientific). For NGF and BDNF, ELISA was performed according to manufacturer's instructions (DY256 for NGF and DY248 for BDNF; duo-set ELISA kits; R&D Systems, Minneapolis, Minnesota, USA).

RNA Extraction, cDNA Synthesis, and Real-Time PCR

Total RNA was extracted from lysates according to the MirvanaParis procedure and rehydrated in 13-μL fresh DEPC-treated and autoclaved MilliQ water. A further RNase-Free DNaseI (2 U/μL; Turbo DNase; Ambion-Thermo, Fisher Scientific, Waltham, MA, USA) treatment was performed before quantitation and assessment of purity. cDNAs were synthesized from 1 μg total RNA (ImProm-II Reverse Transcription System; Promega Corp., Madison, WI, USA) in a

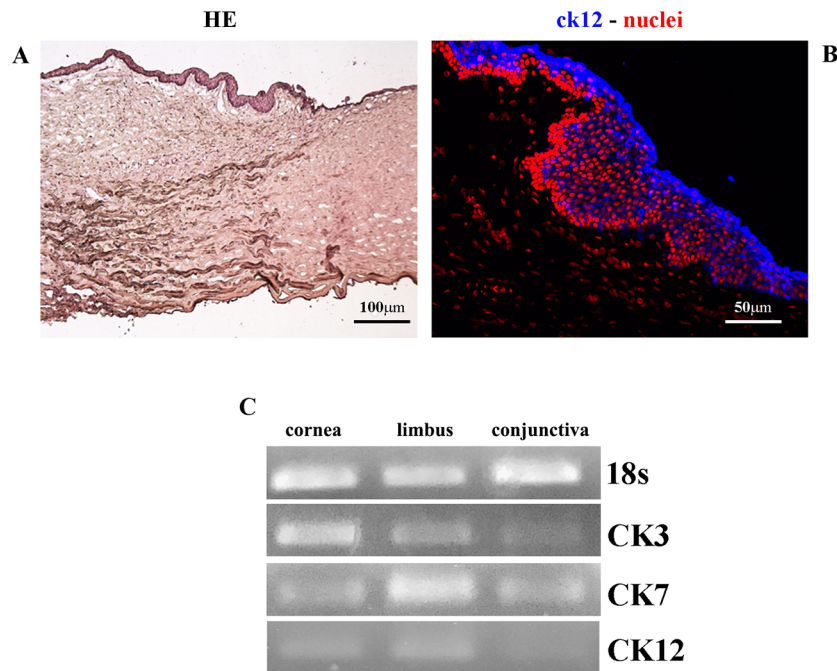


FIGURE 1. (A–C) Characterization of corneoscleral section and tissue extracts. Representative digital acquisitions defining the limbal zone between cornea and conjunctiva: (A) HE overview of a cross-sectional longitudinal tissue sample ($\times 10$ /objective) and (B) Ck12-blue (cornea-limbus marker) immunoreactivity over a red nuclear staining (PI; $\times 40$ /objective). Scale bar are shown in the panels. (C) Amplicons specific for referring (18S) and target (Ck3, Ck7, and Ck12) genes amplified in corneal, limbal, and conjunctival extracts and separated in 2.5% agarose gel.

96-well thermocycler (PqLab Biotechnologie GmbH, Erlangen, Germany) and amplified using the SYBR Green PCR core reagent kit (Applied Biosystems, Foster City, CA) in an eco48 real-time PCR system (Illumina, MA, USA). Pair primers and amplification protocols are shown in Table 1. Single melting curves were verified (Supplementary Fig. S1). Samples were amplified in duplicate and in parallel with negative controls (without template or with total RNA as template). Real cycle numbers (Cq) were recorded from the program (Eco Real-Time PCR System Software v5.0; Illumina), normalized for referring genes run in parallel ($nCq = Cq_{\text{target}} - Cq_{\text{referring}}$) and used for calculating related fold changes (expression ratios expressed as \log_2 -scale from normalized target versus referring gene; REST analysis).

Statistical Analysis

At the beginning, nonparametric Kolmogorov-Smirnov and Shapiro-Wilk tests were carried out for satisfying the Gaussian distribution (GraphPad Prism 5.0; GraphPad Software, Inc., San Diego, CA, USA). For chip array analysis, the specific FI averages (mean \pm SD as produced by the Axon Instruments software) were calculated from replicates (two spots) of not-pooled samples, normalized by subtracting the background signal. Data were provided in an Excel (Microsoft, Redmond, WA, USA) format. The relationship between differentially expressed candidates for each subgroup was calculated by Student's *t*-test comparisons and Bonferroni's correction for 60 targets (StatView II Software; StatView, Barkley, CA, USA). Both two fold-changes (either decrease or increase) and *P* values ≤ 0.00083 (as per 0.05/60 spots/biomarkers tested) were considered cutoffs, whereas $P \leq 0.05$ was considered a significant level among subgroups for ELISA.

RESULTS

An overview of the corneoscleral limbal zone (HE-stained sections) is displayed in Figure 1A. As shown, the typical distribution of the epithelial region alongside the corneoscleral limbal zone is depicted ($\times 10$). Figure 1B shows cross-sectional images of the limbal region immunostained for Ck12 (cy5/blue) over an intense nuclear counterstaining (PI/red) ($\times 40$). As molecular and biochemical analyses were carried out after tissue microdissection, a molecular validation of correct regions by using the cytokeratin expression was carried out at the molecular level. Merely, PCR products amplified from each tissue extract were resolved in agarose gel (Fig. 1C). The related melting curves are reported in Supplementary Figure S1.

Limbal Region Is Populated by AA1 Immunoreactive Mast Cells

TB staining revealed the presence of magenta-purple mast cells in a zone depicted from the limbal region containing radially oriented fibrovascular ridges (palisades of Vogt) ($\times 20$; Fig. 2A) and in a region composed of stromal invaginations ($\times 20$; Fig. 2B). A granule-rich and round-shaped Mast Cell (MC) is shown in Figure 2C ($\times 40$). Immunohistochemistry was used to stain AA1-positive mast cells, as shown in Figure 2D and Figure 2E (brown-DAB labeled; cresyl violet counterstaining; $\times 40$). Insets in Figure 2D and Figure 2E are control isotype staining ($\times 40$; no specific primary antibody). Of interest, AA1 immunolabeled cells were found either degranulated ($\times 40$; Fig. 2F) or intact ($\times 40$; Fig. 2G). Some mast cells were observed in close association to Vogt palisades (intense red nuclear staining; PI) ($\times 20$; Fig. 2H).

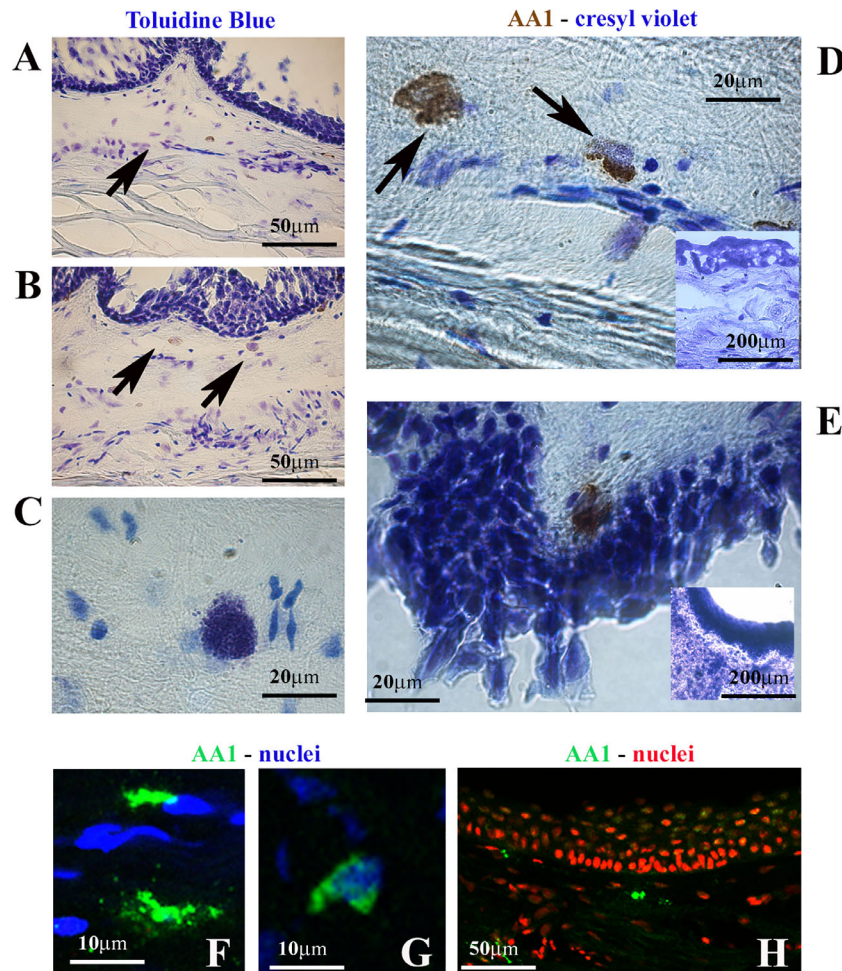


FIGURE 2. (A–G) Immunohistochemical localization of mast cells at limbal zone. Representative digital acquisitions for basal histology (A–E) and immunofluorescent staining (F–H) highlighting the presence of mast cells. (A–C) Low (A, B; $\times 20$) and high (C; $\times 40$) optic field acquisitions from acidic (pH 3) 0.1% toluidine blue–stained sections. Note the presence of “purple-granule” stained mast cells in the limbal segment. (D, E) AA1 immunoreactive cells (brown–dark DAB staining) over a cresyl blue nuclear counterstaining. Note the presence of highly conserved secretory granules in stained cells (D; $\times 40$) and particularly a localization close to dense blue counterstained palisades of Vogt (high nuclear affinity to cresyl violet) (E; $\times 40$). The inset in the panel shows an internal control section from the serial section (absence of first antibody). (F, G) Representative immunofluorescent acquisitions showing AA1 (cy3/green) positive cells ($\times 40$). Note the presence of some partially degranulated mast cells (F) and mast cells with highly conserved (G) secretory granules. (H) A single MC localized in close proximity to dense nuclear palisades.

AA1, cKit Proteins, and Related Transcripts Are Expressed in the Limbal Region

Several AA1 (tryptase)–positive cells were observed at the corneoscleral limbal junction ($\times 20$; Fig. 3A) as well as at the basal epithelial membrane ($\times 40$; Ck12 [blue] staining; Fig. 3B). A clear coexpression of AA1 (tryptase)/CC1 (chymase) immunoreactivity was not observed (data not shown). Double staining for AA1 and cKit is shown in Figure 3C. Almost 4% out of total 12% CD45–positive pan-leucocyte cells were AA1 immunoreactive, as a result of counting positive cells per optic field ($\times 20$; Fig. 3D). The expression of cKit, tryptase (AA1), chymase (CC1), and Fc ϵ RI transcripts in corneal, limbal, and conjunctival extracts is shown in Figure 3E. H3 referring gene was used to normalize the amplifications and provide densitometric analysis specific for AA1 and cKit (Fig. 3F and Fig. 3G, respectively). Relative Expression tool software (REST) analysis from these specific real-time amplifications highlighted the increase

of AA1 transcripts in limbal ($+1.50_{2\log}$ expression ratio) and more consistently in conjunctival ($+2.70_{2\log}$ expression ratio) RNA extracts, with respect to corneal extracts used as control (arbitrary unit). With respect to CC1, unchanged transcript expression was detected in limbal ($+0.30_{2\log}$ expression ratio) and conjunctival ($+1.07_{2\log}$ expression ratio) RNA extracts, as compared with corneal extracts used as control (arbitrary unit).

Limbal Protein Signature Highlights a Selective NCAM1 and ICAM3 as well as BDNF and NT3 Expression

The array chip technology was used to identify different protein expression among limbus, cornea, and conjunctiva (Supplementary Fig. S2A). Volcano plots, representative images of chip membranes, and the array map with the right position of the selected adhesion molecules, cytokines, and

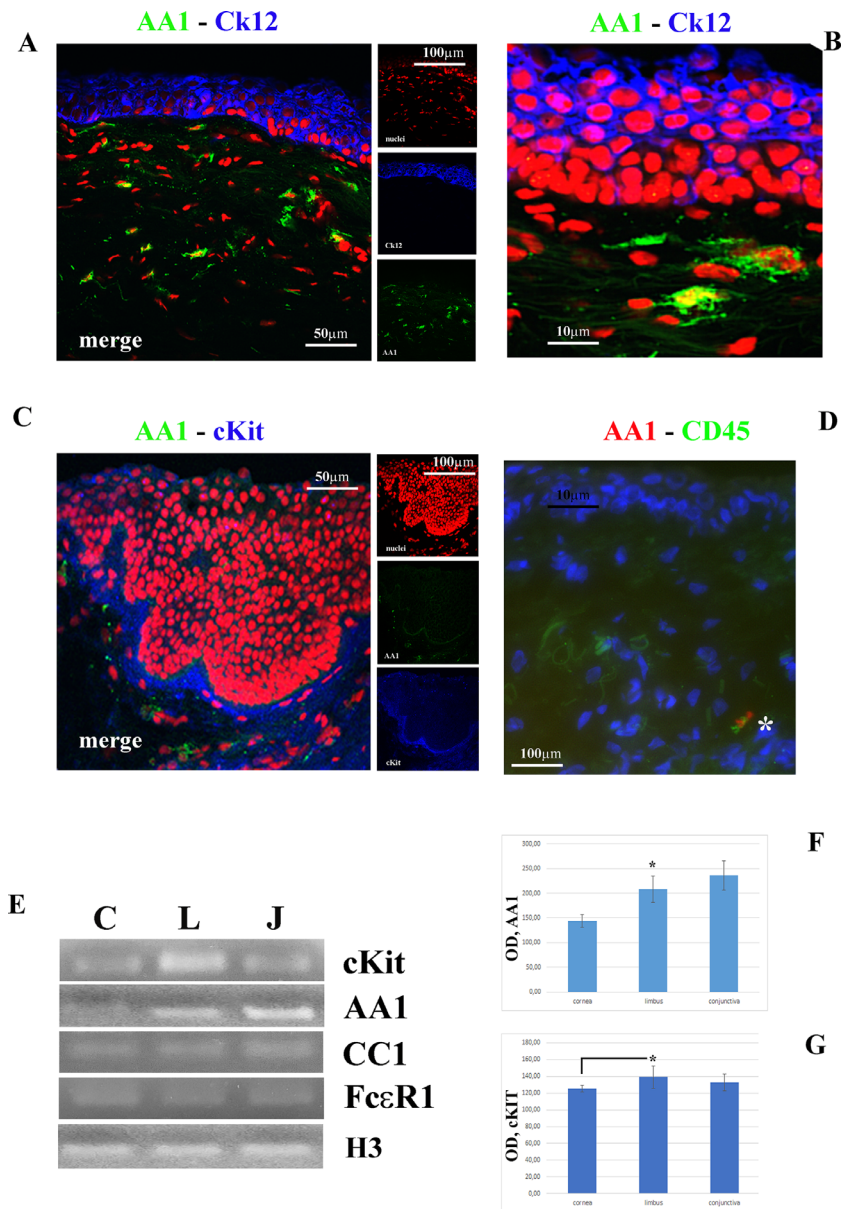


FIGURE 3. (A–E) Characterization of mast cells at the limbal zone. (A, B) Double staining of AA1 (cy2/green) and Ck12 (cy5/blue) over a red nuclear counterstaining (PI; $\times 20$ /objective) and a particular AA1-positive cell close to niches (cy2/green; B). Ck12 stains part of the initial superficial limbal epithelial cells and extend over the corneal epithelium. *White arrows* point at AA1-positive cells. (C, D) Representative double-staining (merge) acquisition respectively for AA1 (cy2/green)–cKit (cy5/blue) and CD45 (cy2/green)–AA1 (cy3/red) over a nuclear counterstaining (DAPI/blue). Single staining is also shown close to the merge, as provided by the Nis software (Nikon). (E, G) Amplicons specific for cKit, AA1, CC1, FcεRI, and H3 are shown with respect to corneal, limbal, and conjunctival extracts. The related densitometric analysis specific for AA1 and cKit is shown in panels F and G, respectively.

growth factors involved in inflammation and tissue remodeling are shown in Supplementary Figures S2B–G. The results of protein array analysis are reported in Table 2, including fold changes and *P* values. A significant upregulation of NCAM1 (aliases NCAM/CD56) and ICAM3 was detected in limbal protein extracts by array chip, as compared to corneal and conjunctival ones ($P < 0.00083$; respectively Fig. 4A and Fig. 4B). In addition, BDNF showed a significant increase in limbal extracts with respect to corneal ones ($P < 0.00083$; Figs. 4B, 4C, 4E), whereas NT3 showed a significant increase in limbal extracts, as compared to both corneal and

conjunctival extracts ($P < 0.005$; Figs. 4B, 4D). No significant differences were observed for EGF and NGF, known to exert both proliferative and survival effects on mast cells and stem cells. EGF protein expression did not change in all extracts (cornea: 2170.630 ± 466.030 Integrated Density (IntDen); limbus: 2388.000 ± 286.160 IntDen; conjunctiva: 2029.630 ± 181.070 IntDen). Similarly, NGF levels in corneal (29.22 ± 5.73 pg/mL), limbal (36.19 ± 2.04 pg/mL), and conjunctival (31.15 ± 2.26 pg/mL) extracts did not change significantly, although a trend to an increase was observed for limbal NGF when compared with the other regions. Comprehensive

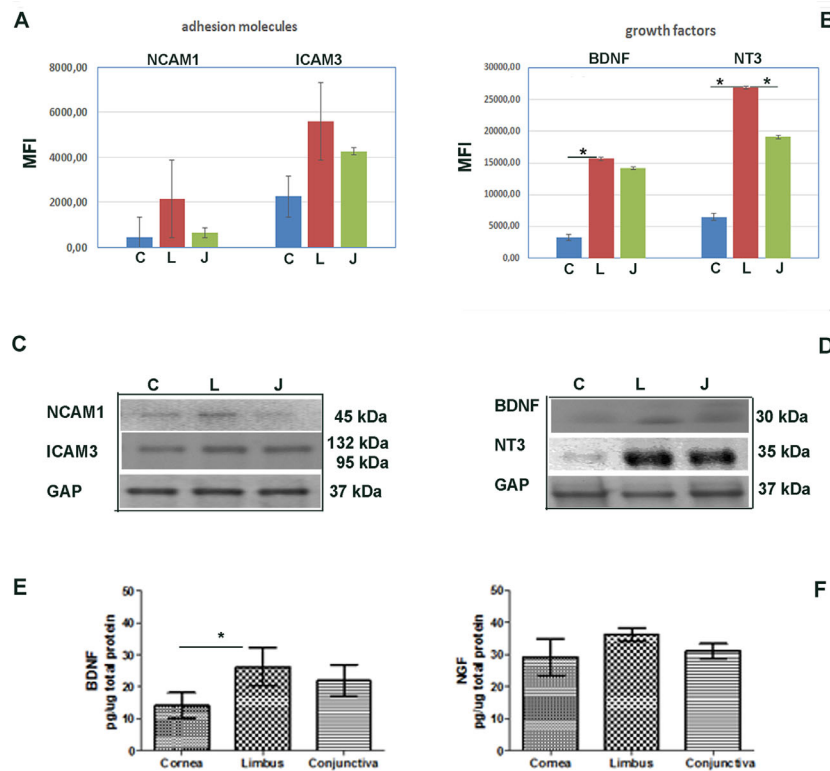


FIGURE 4. (A, B) NCAM-1, ICAM-3, BDNF, NT-3, and NGF are differentially expressed in the limbal zone. Adhesion molecules (NCAM1 and ICAM3; A, C) and growth factor (BDNF-NT3 [B, D, E] and NGF [F]) protein expression in corneal (C), limbal (L), and conjunctival (J) extracts, as confirmed by conventional Western blotting analysis on triplicate repeated experiments (C, D). Note the significant increase of NCAM1 and ICAM3 in limbal extracts (with respect to the other tissue extracts; $P < 0.05$) and BDNF and NT3 in limbal extracts with respect to corneal ones ($P < 0.05$). MFI stands for mean fluorescent intensity, as detected by ImageJ software (National Institutes of Health, Bethesda, MD, USA) on array chip (A, B). BDNF and NGF protein expression (mean \pm SEM) quantified by ELISA and expressed as pg/ μ g total protein (E, F). ANOVA analysis followed by Bonferroni's correction. Asterisks (*) in the histograms point at significant differences between subgroups ($P < 0.05$).

scanned whole immunoblots are shown in Supplementary Figures S3A–E. The results of BDNF- and NGF-specific ELISA are shown respectively in panels Figure 4E and Figure 4F (data normalized for total protein expression and reported as pg/ μ g total protein).

DISCUSSION

By using human corneoscleral specimens, we explored the presence of mast cells in the limbal region, providing additional information on their phenotype and the surrounding microenvironment (protein profiling) with respect to the nearby corneal and conjunctival zones.

The corneoscleral junction has been extensively studied for limbal stem cells' housing and related contribution to ocular surface homeostasis, whereas little attention has been devoted to the other cell types populating this zone and interacting with the microenvironment.^{6,27,28} In previous studies, limbal mast cells were found mainly in close association to vessels.^{16,20,29–31} Mast cell distribution and heterogeneity were later investigated in inflamed and allergic conjunctival samples.^{16,20,29–31} More recently, the involvement of mast cells in retinal disorders was also described.³¹ Consistent evidence indicates that mast cells can work as innate-immune sentinel “gatekeepers” in several systems, including central nervous system, gut, skin, and ocular surface.^{16,20,29–31} Actually, the presence of mast cells

at the corneoscleral junction deserves further attention, and consequently, interest has been devoted to better clarify their potential contribution close to niches.

Therefore, our first attempt was to characterize mast cells in these specimens according to their mucosal (tryptase) and connective (chymase, tryptase, and carboxypeptidases) tissue classification.^{32,33} Our finding confirms the presence of round/oval metachromatic cells in corneoscleral tissues and provides evidence on the presence of tryptase (AA1) immunoreactive mast cells nearby the palisades of Vogt. The morphology of these mast cells appeared either intact (resting) or degranulated (active), suggesting a dynamic contribution of mast cells close to niches. A comparison between intact and degranulated mast cells was not carried out as the degranulation route also might be influenced by tissue sampling and/or handling.³⁴ In fact, low temperatures, freezing/thawing, and some fixatives (Carnoy's fixative, glutaraldehyde, or formaldehyde buffered solutions) might trigger membrane perturbation as well as induce an antidromic nervous stimulation or any other microenvironment insult, resulting in alteration of overall membrane integrity.^{34,35} The observation of only 30% of AA1-positive cells out of total CD45-positive cells suggests the presence of other immune cells populating the limbal junction.^{31,36} The specific expression of tryptase (AA1) and the almost undetectable immunoreactivity for chymase (CC1) and chymase/tryptase coexpression, confirmed by

TABLE 2. Protein Array

Targets	Limbus vs. Conjunctiva		Limbus vs. Cornea	
	FC	p Value	FC	p Value
IL-1 β	1.34	0.3507	1.21	0.4519
IL-4	1.67	0.2013	1.21	0.4554
IL-6	-1.11	0.4600	-3.18	0.2918
IL-8	1.20	0.3005	1.14	0.3963
IL-10	1.01	0.9773	-1.02	0.9627
IL-11	-1.61	0.5034	-1.94	0.4824
IL-12p40	1.47	0.2023	1.21	0.4952
IL-12p70	1.16	0.7592	1.14	0.7275
IL-21	1.67	0.4431	-1.39	0.5768
TNF- α	1.32	0.0807	1.42	0.0822
TNF- β	1.25	0.3993	-1.22	0.4907
IFN-gamma	1.71	0.3100	1.12	0.7730
Eotaxin	1.17	0.8322	-2.15	0.4496
Eotaxin-2	-1.12	0.7081	-4.72	0.3687
TIMP-1	1.52	0.1779	1.07	0.8310
TIMP-2	1.51	0.5238	1.28	0.6273
TIMP-3	-1.52	0.4901	-6.81	0.2286
TIMP-4	1.48	0.3124	-1.41	0.5638
VCAM-1	1.31	0.6092	-1.08	0.9180
NCAM-1	3.31	0.2030	4.98	0.0146
ICAM-1	-2.57	0.4633	-2.51	0.4176
ICAM-2	-1.38	0.3230	-1.08	0.8508
ICAM-3	1.31	0.5123	2.48	0.0235
Osteopontin	1.80	0.2496	1.26	0.6122
Insulin	-1.38	0.5888	-2.02	0.0843
EPO	-2.15	0.2689	1.20	0.7516
IL-17	2.02	0.1511	4.51	0.0821
RANTES	1.36	0.5506	-1.11	0.8038
TACE	-4.00	0.2842	1.06	0.8204
MIP-1alpha	1.17	0.7004	1.29	0.3923
MIP-1 β	-1.65	0.4830	-1.29	0.8156
MIP-1delta	-1.18	0.7884	-1.00	0.9944
MIP-3alpha	-1.71	0.2143	-1.51	0.5588
MIP-3 β	-1.47	0.4950	-1.32	0.7537
TLR2	1.55	0.4381	-1.03	0.9534
MCP-1	-3.33	0.2908	-1.33	0.4754
IL-13	-1.76	0.5105	-2.74	0.2507
IP-10	1.26	0.4451	-1.02	0.9377
GDNF	2.06	0.0841	1.22	0.4200
BDNF	1.10	0.8272	4.86	0.0022
NT-3	1.41	0.2073	4.17	0.0002
NT-4	-1.04	0.9474	1.20	0.6656
G-CSF	1.72	0.0538	1.48	0.1572
M-CSF	1.25	0.5918	1.15	0.7142
PIGF	1.59	0.4691	-1.09	0.8628
β NGF	1.26	0.5971	1.04	0.8884
VEGF	-1.34	0.6389	1.58	0.3444
TGF- β 1	1.38	0.6028	-1.04	0.9638
IGF-I	-1.04	0.9301	-3.06	0.3342
PDGF-BB	3.54	0.3545	1.13	0.8217
β FGF	-1.68	0.2767	-1.20	0.6983
EGF	1.18	0.6587	1.10	0.7048
sTNF-RI	3.20	0.1019	2.07	0.2454
sTNF-RII	1.31	0.5092	1.39	0.4082
VEGF-RI	1.35	0.4139	1.25	0.5605
FAS-L	1.60	0.1323	3.58	0.0825
VEGF-RII	1.88	0.4246	2.45	0.2903
PEDF	1.05	0.7985	1.67	0.1791
β 2-MG	1.25	0.1404	1.44	0.1156
Albumin	1.06	0.8038	-1.12	0.4317

Notes: FC, fold changes; pValue, a $p < 0.0083$ was considered significant according to a pValue of 0.05 and the total number of targets (60). An increase/decrease in 2 FC was in this test. β 2M, beta2 Microglobulin.

Note that bold represents significant fold changes while italic bold highlights the significant pValue.

epifluorescent and molecular analysis, would suggest a “potential” tryptase contribution in the local mast cell–driven tissue homeostasis and parainflammation.^{31,36} As shown elsewhere, tryptase takes part in some physiologic activities (tissue airway homeostasis, vascular relaxation and contraction, gastrointestinal smooth muscle activity, intestinal transport, and coagulation pathway) by degrading some components of the cellular matrix (merely fibronectin), regulating cell trafficking and taking part in local homeostasis.^{37–40,41} Galli and coworkers⁴² highlighted the concept that mast cells can function as immunoregulatory cells, prospecting the concept of OFF/resting or ON/degranulating functional configurations. Although increased levels of systemic/local tryptase are frequently associated with Th2-driven chronic inflammatory and fibrotic ocular conditions, the presence of tryptase by itself does not represent an exclusive indication of anaphylaxis and/or allergy.^{30,41,43,44} Mast cell survival inside tissues is guaranteed by several cytokines and growth factors and particularly by cKit and Stem Cell Factor (SCF). The results on cKit and SCF demonstrated no significant changes in limbal expression with respect to the nearby areas. This result is in line with previous studies suggesting that cKit is not restricted to mast cells.^{16,20,29–31} Both IgE-dependent and no IgE-dependent activations drive mast cell activity and particularly degranulation.^{16,20,29–31} The high-affinity IgE receptor (Fc ϵ RI) was investigated at both biochemical and molecular levels. On the contrary, Fc ϵ RI surface receptor was not detected by immunofluorescence and only weakly expressed by molecular analysis, opening the question of whether no IgE-dependent mast cell activity is close to the niches. According to literature, Fc ϵ RI is weakly expressed upon a nonallergic background and works as an inducible short-term life receptor in cultures exposed to IgE.⁴⁵

Mast cells are tissue-sited and long-living cells exerting a prompt early release of preformed mediators and a quick granule renewal to ensure an exhaustive protection.^{31,46} This no IgE-dependent release of mediators can characterize the microenvironment at the host-environment interface and can allow a prompt response to tissue perturbations by activating a selective response, including the IgE-dependent one.^{20,30,33} For this dynamic activity, mast cells are defined as a “source of nourishment” for surrounding tissues and tissue-resident strategic actors in both innate (life-saving host response to bacterial infections) and adaptive (Th2/IgE-mediated and chronic Th1/autoimmune reactions) responses.^{23,24,47} Participation in parainflammation and likewise inflammaging has been described recently.^{30,33,45,48,49} So, mast cell recruitment at stem cell niches might find an attractive explanation also in the protective efforts to guarantee physiologic processes (homeostasis) by means of a no-IgE-dependent route (NGF, TGF β 1, and SCF).^{25,31,33,42,45,48,50–56} Our protein array analysis showed that the limbal protein signature did not match completely with those of neighboring cornea and conjunctiva. This differential protein expression, highlighting NCAM1, ICAM3, BDNF, and NT3, might be consistent with a stem cell–enriched microenvironment.^{1–3,6} Particularly, the higher expression of NCAM-ICAM3 (adhesion molecules) with respect to cornea and conjunctiva ($P < 0.05$) and, to a lesser extent, of BDNF-NT3 with respect to cornea ($P < 0.05$) and finally the no significant changes in EGF and NGF with respect to both corneal and conjunctival extracts would be in line with the growth/survival, homeostatic, and cell trafficking activities required for regulating this highly

vascularized and innervated area.^{44,49,57–59} By the way, we cannot confirm that these factors represent a unique mast cell derivation, as epithelial, stromal, immune, and even stem cells can also release and respond to the above-reported factors.⁵⁹

Overall, the interest in the corneal junction has gradually increased due to continuous corneal regeneration to guarantee ocular surface unit homeostasis, avoiding severe ocular surface impairments (conjunctivalization, corneal ulcers, and stromal scarring) and the related applications in surgery.^{12,28,58,60–65} Altogether, genetic, epigenetic, and other endogenous states might influence the local microenvironment and likewise stem cell behavior, triggering the development or even affecting the persistence and/or exacerbation of severe ocular diseases.^{62,66} In this study, we highlight an interesting aspect of mast cells in supporting stem cell refeeding through a potential no-IgE-dependent contribution. As reported elsewhere, mast cells can promote mesenchymal stem cell proliferation/migration as well as inhibit mesenchymal stem cell differentiation into myofibroblasts (myoFBs).⁶⁷ A limit of this study is represented by the absence of direct “in vitro” data showing the release of mast cell mediators for stem cell proliferation/survival. Indeed, the absence of FcεRI expression (the receptor responsible for the IgE-dependent route) cannot definitely exclude the presence of a potential IgE-mediated mast cell response to eventual allergic insults with release of the Th2 subset (IL4, IL10, TGFβ1, and stat5).^{45,66,68,69}

Overall, the data herein reported focus on a future consideration of the limbal zone in terms of a complex integrated structural (epithelial cells and fibroblasts) and immune (mast cells, neutrophils, and lymphocytes) cell compartment sustaining the stem cell niches. Although the surgical practice represents a successful routine approach, a better understanding of cell subtypes and microenvironment at this transition zone might increase the strategies of corneal epithelial repair and ocular surface homeostasis in the field of personalized medicine and individualized therapy.^{14,30,70}

Acknowledgments

The authors thank Fondazione Roma (Italy) for continuous intramural support and encouragement. Many thanks to Egidio Stigliano (Department of Pathology, Fondazione Policlinico Universitario A. Gemelli, Catholic University School of Medicine, Rome, Italy) for supervising the limbal, corneal, and conjunctival dissection under stereomicroscope and to Ramona Marino (University Campus BioMedico, Rome, Italy) for contributions in sample sectioning. The study was the extension of laureate training (Giulia Midena and Olivia Florio; University Campus BioMedico, Rome, Italy).

Partially supported by the Italian Ministry of Health (RC263502 to IRCCS-Fondazione Bietti). Also supported by research project BBMRI_CZ LM2015089 and by Progres-Q25 (KJ).

Disclosure: **A. Micera**, None; **K. Jirsova**, None; **G. Esposito**, None; **B.O. Balzamino**, None; **A. Di Zazzo**, None; **S. Bonini**, None

References

- Pellegrini G, Traverso CE, Franzi AT, Zingirian M, Cancedda R, De Luca M. Long-term restoration of damaged corneal surfaces with autologous cultivated corneal epithelium. *Lancet*. 1997;349:990–993.
- Pellegrini G, Golisano O, Paterna P, et al. Location and clonal analysis of stem cells and their differentiated progeny in the human ocular surface. *J Cell Biol*. 1999;145:769–782.
- Di Iorio E, Barbaro V, Ruzza A, Ponzin D, Pellegrini G, De Luca M. Isoforms of DeltaNp63 and the migration of ocular limbal cells in human corneal regeneration. *Proc Natl Acad Sci USA*. 2005;102:9523–9528.
- Umamoto T, Yamato M, Nishida K, Yang J, Tano Y, Okano T. Limbal epithelial side-population cells have stem cell-like properties, including quiescent state. *Stem Cells*. 2006;24:86–94.
- Zhang Y, Sun H, Liu Y, et al. The limbal epithelial progenitors in the limbal niche environment. *Int J Med Sci*. 2016;13:835–840.
- Dua HS, Azuara-Blanco A. Limbal stem cells of the corneal epithelium. *Surv Ophthalmol*. 2000;44:415–425.
- Holland EJ. Epithelial transplantation for the management of severe ocular surface disease. *Trans Am Ophthalmol Soc*. 1996;94:677–743.
- Haagdorens M, Ilse Van Acker S, Van Gerwen V, et al. Limbal stem cell deficiency: current treatment options and emerging therapies. *Stem Cells Int*. 2016;2016:9798374.
- Tsai RJ, Li LM, Chen JK. Reconstruction of damaged corneas by transplantation of autologous limbal epithelial cells. *N Engl J Med*. 2000;343:86–93.
- Dua HS, Joseph A, Shanmuganathan VA, Jones RE. Stem cell differentiation and the effects of deficiency. *Eye (Lond)*. 2003;17:877–885.
- Pellegrini G, Dellambra E, Golisano O, et al. p63 identifies keratinocyte stem cells. *Proc Natl Acad Sci USA*. 2001;98:3156–3161.
- Pellegrini G, Rama P, De Luca M. Vision from the right stem. *Trends Mol Med*. 2011;17:1–7.
- Rama P, Bonini S, Lambiase A, et al. Autologous fibrin-cultured limbal stem cells permanently restore the corneal surface of patients with total limbal stem cell deficiency. *Transplantation*. 2001;72:1478–1485.
- Dua HS, Miri A, Said DG. Contemporary limbal stem cell transplantation—a review. *Clin Exp Ophthalmol*. 2010;38:104–117.
- Kinoshita S, Kiorpes TC, Friend J, Thoft RA. Limbal epithelium in ocular surface wound healing. *Invest Ophthalmol Vis Sci*. 1982;23:73–80.
- McMenamin PG, Morrison SM, McMenamin C. Immunomorphologic studies of mast cell heterogeneity, location, and distribution in the rat conjunctiva. *J Allergy Clin Immunol*. 1996;97:1375–1386.
- Gipson IK. The ocular surface: the challenge to enable and protect vision: the Friedenwald lecture. *Invest Ophthalmol Vis Sci*. 2007;48:4391–4398.
- Sahu SK, Mittal SK, Foulsham W, Li M, Sangwan VS, Chauhan SK. Mast cells initiate the recruitment of neutrophils following ocular surface injury. *Invest Ophthalmol Vis Sci*. 2018;59:1732–1740.
- Royer DJ, Zheng M, Conrady CD, Carr DJ. Granulocytes in ocular HSV-1 infection: opposing roles of mast cells and neutrophils. *Invest Ophthalmol Vis Sci*. 2015;56:3763–3775.
- Metcalf DD, Baram D, Mekori YA. Mast cells. *Physiol Rev*. 1997;77:1033–1079.
- Kumar V, Sharma A. Mast cells: emerging sentinel innate immune cells with diverse role in immunity. *Mol Immunol*. 2010;48:14–25.
- Micera A, Puxeddu I, Aloe L, Levi-Schaffer F. New insights on the involvement of nerve growth factor in allergic inflammation and fibrosis. *Cytokine Growth Factor Rev*. 2003;14:369–374.
- Galli SJ, Tsai M. Mast cells: versatile regulators of inflammation, tissue remodeling, host defense and homeostasis. *J Dermatol Sci*. 2008;49:7–19.

24. Galli SJ. The mast cell-IgE paradox: from homeostasis to anaphylaxis. *Am J Pathol.* 2016;186:212–224.
25. Piliponsky AM, Romani L. The contribution of mast cells to bacterial and fungal infection immunity. *Immunol Rev.* 2018;282:188–197.
26. Micera A, Di Zazzo A, Esposito G, Sgrulletta R, Calder VL, Bonini S. Quiescent and active tear protein profiles to predict vernal keratoconjunctivitis reactivation. *Biomed Res Int.* 2016;2016:9672082.
27. Chen Z, de Paiva CS, Luo L, Kretzer FL, Pflugfelder SC, Li DQ. Characterization of putative stem cell phenotype in human limbal epithelia. *Stem Cells.* 2004;22:355–366.
28. Welle M. Development, significance, and heterogeneity of mast cells with particular regard to the mast cell-specific proteases chymase and tryptase. *J Leukoc Biol.* 1997;61:233–245.
29. Church MK, McGill JI. Human ocular mast cells. *Curr Opin Allergy Clin Immunol.* 2002;2:419–422.
30. Xie Y, Zhang H, Liu S, et al. Mast cell activation protects cornea by promoting neutrophil infiltration via stimulating ICAM-1 and vascular dilation in fungal keratitis. *Sci Rep.* 2018;8:8365
31. Heib V, Becker M, Taube C, Stassen M. Advances in the understanding of mast cell function. *Br J Haematol.* 2008;142:683–694.
32. Longley BJ, Tyrrell L, Lu S, Ma Y, Klump V, Murphy GF. Chronically c-kit-stimulated clonally-derived human mast cells show heterogeneity in different tissue microenvironments. *J Invest Dermatol.* 1997;108:792–796.
33. Church MF, Levi-Schaffer F. The human mast cells. *J Allergy Clin Immunol.* 1997;99:155–160.
34. Lampe M, Kiernan JA. Degranulation of dermal mast cells: effects of fixation and of antidromic nervous impulses on two histochemically identified cell-types. *Arch Dermatol Res.* 1976;257:125–129.
35. Lambiase A, Micera A, Bonini S. Multiple action agents and the eye: do they really stabilize mast cells? *Curr Opin Allergy Clin Immunol.* 2009;9:454–465.
36. Huber M, Cato ACB, Ainooson GK, et al. Regulation of the pleiotropic effects of tissue resident mast cells. *J Allergy Clin Immunol.* 2019;144:S31–S45.
37. Pejler G, Abrink M, Ringvall M, Wernersson S. Mast cell proteases. *Adv Immunol.* 2007;95:167–255.
38. Vartio T, Seppa H, Vaheri A. Susceptibility of soluble and matrix fibronectins to degradation by tissue proteases, mast cell chymase and cathepsin G. *J Biol Chem.* 1981;256:471–477.
39. Lohi J, Harvima I, Keski-Oja J. Pericellular substrates of human mast cell tryptase 72,000 dalton gelatinase and fibronectin. *J Cell Biochem.* 1992;50:337–349.
40. Hershkoviz R, Preciado-Patt L, Lider O, Fridkin M, Mekori YA. Mast cell adhesion to extracellular matrix: local effects of acute phase reactants. *Int Arch Allergy Immunol.* 1997;113:295–296.
41. Payne V, Kam PC. Mast cell tryptase: a review of its physiology and clinical significance. *Anaesthesia.* 2004;59:695–703.
42. Galli SJ, Kalesnikoff J, Grimbaldston MA, Piliponsky AM, Williams CM, Tsai M. Mast cells as “tunable” effector and immunoregulatory cells: recent advances. *Annu Rev Immunol.* 2005;23:749–786.
43. Yao L, Baltatzis S, Zafirakis P, Livir-Rallatos C, et al. Human mast cell subtypes in conjunctiva of patients with atopic keratoconjunctivitis, ocular cicatricial pemphigoid and Stevens-Johnson syndrome. *Ocul Immunol Inflamm.* 2003;11:211–222.
44. Levi-Schaffer F, Micera A, Zamir E, et al. Nerve growth factor and eosinophils in inflamed juvenile conjunctival nevus. *Invest Ophthalmol Vis Sci.* 2002;43:1850–1856.
45. Demetri GD. Targeting c-kit mutations in solid tumors: scientific rationale and novel therapeutic options. *Semin Oncol.* 2001;28:19–26.
46. Frossi B, De Carli M, Pucillo C. The mast cell: an antenna of the microenvironment that directs the immune response. *J Leukoc Biol.* 2004;75:579–585.
47. Sabatino F, Di Zazzo A, De Simone L, Bonini S. The intriguing role of neuropeptides at the ocular surface. *Ocul Surf.* 2017;15:2–14.
48. Aloe L, Levi-Montalcini R. Mast cells increase in tissues of neonatal rats injected with the nerve growth factor. *Brain Res.* 1977;133:358–366.
49. Leon A, Buriani A, Dal Toso R, et al. Mast cells synthesize, store, and release nerve growth factor. *Proc Natl Acad Sci USA.* 1994;91:3739–3743.
50. Cardamone C, Parente R, Feo GD, Triggiani M. Mast cells as effector cells of innate immunity and regulators of adaptive immunity. *Immunol Lett.* 2016;178:10–14.
51. Greiner JV, Peace DG, Baird RS, Allansmith MR. Effects of eye rubbing on the conjunctiva as a model of ocular inflammation. *Am J Ophthalmol.* 1985;100:45–50.
52. Yazdanpanah G, Jabbehdari S, Djaliliana AR. Limbal and corneal epithelial homeostasis. *Curr Opin Ophthalmol.* 2017;28:348–354.
53. Busanello A, Santucci D, Bonini S, Micera A. Environmental impact on ocular surface disorders: possible epigenetic mechanism modulation and potential biomarkers. *Ocul Surf.* 2017;15:680–687.
54. Yu Y, Blokhuis BR, Garssen J, Redegeld FA. Non-IgE mediated mast cell activation. *Eur J Pharmacol.* 2016;778:33–43.
55. Sgrulletta R1, Bonini S, Lambiase A, Bonini S. Allergy and infections: long-term improvement of vernal keratoconjunctivitis following viral conjunctivitis. *Eur J Ophthalmol.* 2006;16:470–473.
56. Bonini S, Lambiase A, Sgrulletta R, Bonini S. Allergic chronic inflammation of the ocular surface in vernal keratoconjunctivitis. *Curr Opin Allergy Clin Immunol.* 2003;3:381–387.
57. Vega E, Rudolph MI. Characterization of oxytocin receptors and serotonin transporters in mast cells. *Endocrine.* 2002;18:167–172.
58. Tseng SCG, He H, Zhang S, Chen SY. Niche regulation of limbal epithelial stem cells: relationship between inflammation and regeneration. *Ocul Surf.* 2016;14:100–112.
59. Saito H, Okajima F, Molski TF, Sha'afi RI, Ui M, Ishizaka T. Effect of cholera toxin on histamine release from bone marrow-derived mouse mast cells. *Proc Natl Acad Sci USA.* 1988;85:2504–2508.
60. Rama P, Matuska S, Paganoni G, Spinelli A, De Luca M, Pellegrini G. Limbal stem-cell therapy and long-term corneal regeneration. *N Engl J Med.* 2010;363:147–155.
61. Schlötzer-Schrehardt U, Kruse FE. Identification and characterization of limbal stem cells. *Exp Eye Res.* 2005;81:247–264.
62. Bonini S, Micera A, Ioviengo A, Lambiase A, Bonini S. Expression of Toll-like receptors in healthy and allergic conjunctiva. *Ophthalmology.* 2005;112:1528; discussion 1548–1549.
63. Bonini S, Lambiase A, Sacchetti M, Bonini S. Cytokines in ocular allergy. *Int Ophthalmol Clin.* 2003;43:27–32.
64. Sangwan VS, Jain V, Vemuganti GK, Murthy SI. Vernal keratoconjunctivitis with limbal stem cell deficiency. *Cornea.* 2011;30:491–496.
65. Sacchetti M, Rama P, Bruscolini A, Lambiase A. Limbal stem cell transplantation: clinical results, limits, and perspectives. *Stem Cells Int.* 2018;2018:8086269.
66. Saboo US, Basu S, Tiwari S, Mohamed A, Vemuganti GK, Sangwan VS. Clinical and cytologic evidence of limbal stem cell deficiency in eyes with long-standing vernal keratoconjunctivitis. *Asia Pac J Ophthalmol (Phila).* 2013;2:88–93.

67. Nazari M, Ni NC, Lüdke A, et al. Mast cells promote proliferation and migration and inhibit differentiation of mesenchymal stem cells through PDGF. *J Mol Cell Cardiol.* 2016;94:32–42.
68. Iwamoto T, Smelser GK. Electron microscope studies on the mast cells and blood and lymphatic capillaries of the human corneal limbus. *Invest Ophthalmol* 1965;4:815–34.
69. Irani AA, Butrus SI, Tabbara KF, Schwartz LB. Human conjunctival mast cells: distribution of MCr and MC-rc in vernal conjunctivitis and giant papillary conjunctivitis. *J Allergy Clin Immunol* 1990;86:34–40.
70. Lavker RM, Tseng SC, Sun TT. Corneal epithelial stem cells at the limbus: looking at some old problems from a new angle. *Exp Eye Res.* 2004;78:433–446.